^{6}Li Magic-Angle Spinning (MAS) NMR Study of Electron Correlations, Magnetic Ordering, and Stability of Lithium Manganese(III) Oxides

Young Joo Lee and Clare P. Grey*

Department of Chemistry, State University of New York at Stony Brook, Stony Brook, New York 11794-3400

Received June 8, 2000. Revised Manuscript Received October 3, 2000

Three different lithium manganese(III) oxides (the orthorhombic $LiMnO_2$ phase, monoclinic layered $LiMnO_2$ and tetragonal $Li_2Mn_2O_4$) were studied with ^{6}Li magic-angle spinning (MAS) NMR spectroscopy. Much smaller shifts of 36−143 ppm are observed for the Mn(III) phases, in comparison to the other lithium manganese oxides with manganese oxidation states varying from +3.5 to +4. The NMR shift of this system is governed by the Fermi-contact interaction and consequently, is controlled by the lithium local environment. For orthorhombic $LiMnO_2$, one resonance at 36 ppm is observed between −39 and 283 °C and a single resonance at −5 ppm is seen below −39 °C, indicating a magnetic phase transition involving a change from short-range electronic correlations to long-range antiferromagnetic ordering. The ^{6}Li NMR shift of the resonances of the monoclinic and tetragonal phases show very little change with temperature in the range studied (−136 to 283 °C), implying that short-range antiferromagnetic interactions between Mn cations also exist for these phases. No evidence for a magnetic phase transition to three-dimensional ordering, however, is observed. Two different lithium sites are identified in $Li_2Mn_2O_4$, which are assigned to lithium on the 8c octahedral and 4a tetrahedral sites. Samples with lithium on the 8c site only are obtained using mild synthesis conditions, whereas occupation of both sites is obtained with more stringent conditions or at high temperatures.

Introduction

The layered compounds $LiMO_2$ (with M = Co, Ni, V, Cr), are isostructural with α-$NaFeO_2$, crystallizing in the rhombohedral space group $R3m$.[1−4] Lithium cations can be deintercalated and intercalated reversibly from the Co and Ni phases at ∼4 V. Thus, these materials have been studied extensively as possible cathode materials for lithium rechargeable batteries, $LiCoO_2$ being used commercially in this application.[5] Nevertheless, the high cost and toxicity of these materials have prompted searches for replacement materials. Lithium manganese oxides represent attractive substitutes from an economical and environmental standpoint and many studies have focused on synthesizing the pure and doped versions of the layered $LiMnO_2$ phase, and improving their stability following multiple charging cycles.[6−9]

$LiMnO_2$ adopts the orthorhombic ($Pmmn$) structure in its most stable state.[10,11] This crystal structure is composed of alternating layers of Li and Mn octahedra; however, the layers are distorted, forming a zigzag stacking pattern. Recently, the metastable layered $LiMnO_2$ phase has been synthesized by an ion-exchange route from α-$NaMnO_2$[6] and by a hydrothermal reaction of Mn_2O_3 in a mixed alkaline solution such as LiOH (or LiCl) and KOH.[8] Because of the Jahn−Teller distortion around the d^4 Mn^{3+} ion ($t_{2g}^3e_g^1$), the structure adopts a monoclinic space group ($C2/m$), rather than the rhombohedral space group observed for $LiCoO_2$. As in the $LiMO_2$ (M = Ni and Co) materials, this compound contains alternating layers of octahedrally coordinated Li^+ and Mn^{3+} ions, formed by filling alternate planes of octahedral sites in a close-packed array of oxygen anions. A third $LiMnO_2$ phase, tetragonal $Li_2Mn_2O_4$ (*t*-$Li_2Mn_2O_4$), can be attained by intercalation of lithium cations into $LiMn_2O_4$ through either electrochemical or chemical lithiation.[12,13] This phase adopts the space group $I4_1/amd$. There has been some controversy concerning the occupancy of lithium in this structure. David et al. suggested that electrostatic repulsion between Mn

* To whom correspondence should be addressed.

(1) Johnston, W. D.; R. R. Heikes; Sestrich, D. *J. Phys. Chem. Solids* **1958**, *7*, 1.
(2) Goodenough, J. B.; Wickham, D. G.; Croft, W. J. *J. Appl. Phys.* **1958**, *29*, 382.
(3) Kobayashi, K.; Kosuge, K.; Kachi, S. *Mater. Res. Bull* **1969**, *4*, 95.
(4) Rüdorff, W.; Becker, H. *Z. Naturforsch.* **1954**, *9*, 614.
(5) Nagaura, T.; Tazawa, K. *Prog. Batteries Sol. Cells* **1990**, *9*, 209.
(6) Armstrong, A. R.; Bruce, P. G. *Nature* **1996**, *381*, 499.
(7) Capitaine, F.; Gravereau, P.; Delmas, C. *Solid State Ionics* **1996**, *89*, 197.
(8) Tabuchi, M.; Ado, K.; Kobayashi, H.; Kageyama, H.; Masquelier, C.; Kondo, A.; Kanno, R. *J. Electrochem. Soc.* **1998**, *145*, L49.
(9) Jang, Y.-I.; Huang, B.; Chiang, Y.-M.; Sadoway, D. R. *Electrochem. Solid-State Lett.* **1998**, *1*, 13.
(10) Hoppe, V. R.; Brachtel, G.; Jansen, M. *Z. Anorg. Allg. Chem.* **1975**, *417*, 1.
(11) Dittrich, V. G.; Hoppe, R. *Z. Anorg. Allg. Chem.* **1969**, *368*, 262.
(12) Thackeray, M. M.; David, W. I. F.; Bruce, P. G.; Goodenough, J. B. *Mater. Res. Bull.* **1983**, *18*, 461.
(13) David, W. I. F.; Thackeray, M. M.; de Picciotto, L. A.; Goodenough, J. B. *J. Solid State Chem.* **1987**, *67*, 316.

10.1021/cm000469t CCC: $19.00
Published on Web 11/22/2000

in the 8d octahedral site and Li in the 8c octahedral site of the spinel structure results in the occupancy of both the tetrahedral and octahedral sites.[13] However, a recent report by Wills et al. showed that the lithium cations reside in 8c octahedral site only (i.e., the 16c site of the cubic structure).[14]

Lithium manganates have also been studied for their magnetic and structural properties, interest in the former resulting in part due to the frustrated nature of some of the spins in the manganese sublattices. The magnetic properties of orthorhombic $LiMnO_2$ (*o*-$LiMnO_2$) have been investigated using magnetic susceptibility (χ) measurements and neutron diffraction.[15] Curie−Weiss behavior was not observed until above 600 K, and two-dimensional (2-D) spin correlations were shown to be important in the temperature regime below 600 K. A magnetic phase transition from 2-D short-range ordering to three-dimensional (3-D) long-range ordering is seen at 261.5 K. A very large, negative Weiss constant of −1056 K was measured, indicating strong antiferromagnetic correlations between Mn^{3+} cations in this structure. First-principle calculations showed that these strong antiferromagnetic interactions stabilize the orthorhombic structure over the layered structure.[16] Similar magnetic behavior (i.e., 2-D magnetic correlations and a non-Curie−Weiss Law dependence of χ^{-1} with temperature) was observed for *t*-$Li_2Mn_2O_4$ at temperatures close to room temperature.[14] However, no evidence for long-range magnetic order was discerned even down to 1.6 K. For monoclinic $LiMnO_2$ (*m*-$LiMnO_2$), calculations suggest that antiferromagnetic couplings within the MnO_6 layers exist, which are dominated by one-dimensional (1-D) interactions between Mn atoms in chains along the *b*-axis.[17] Magnetic susceptibility data of *m*-$LiMnO_2$ suggest that antiferromagnetic ordering occurs below 250 K.[8] Metal (e.g., Al, Co, Cr)-doping of $LiMnO_2$ stabilizes the monoclinic layered structure[9,18,19] and the magnetic susceptibility of $LiAl_{0.05}Mn_{0.95}O_2$ has been found to follow the Curie−Weiss law above 300 K.[20] A large, negative value of the Weiss constant was observed for the Al-doped phase, again indicating that antiferromagnetic interactions are present. Spin-glass behavior was, however, observed at low temperatures, indicating that long-range antiferromagnetic ordering does not occur in this system.

^{6}Li and ^{7}Li NMR spectroscopy are ideal methods to probe the lithium local structures and electronic states of nearby cations. The interactions between the nuclear and unpaired electron spins associated with the manganese paramagnets complicate the acquisition and interpretation of NMR spectra, but should, at least in theory, provide information concerning the nature of the electronic spin states present in these systems. Recent results from a number of groups have shown that relatively high-resolution spectra can be obtained from these classes of materials. For example, ^{7}Li NMR results on $LiMn_2O_4$ and Li_2MnO_3 have been analyzed in terms of transferred hyperfine coupling between the lithium nuclei and d electron of manganese.[21,22] We showed that the shifts of the manganese(IV) compounds can be readily explained by considering the Li−O−Mn bond angles, and thus the size of the interaction between the Mn^{4+} t_{2g} orbitals, the oxygen p orbitals, and the lithium 2s orbitals. Curie-like temperature dependences were observed for the $LiMn_2O_4$ phases, and the temperature-dependent behavior of the ^{7}Li NMR spectra was observed to be correlated with the magnetic properties.[23] Charge ordering of the Mn^{3+} and Mn^{4+} ions was examined below the cubic-to-tetragonal transition temperature by magic-angle spinning (MAS) NMR[21] and below the Néel temperature by wide-line NMR.[24] ^{7}Li NMR spectra of $LiMn_2O_4$ lithiated at ∼3 V to form $Li_2Mn_2O_4$ have also been published.[25]

^{7}Li NMR spectroscopy is affected by large quadrupolar interactions and dipolar couplings (to the nuclear and the electronic spins), resulting in broadening, and multiple spinning sidebands under MAS conditions. ^{6}Li possesses a much smaller quadrupole moment than ^{7}Li. In addition, the smaller gyromagnetic ratio of ^{6}Li and the consequently smaller dipolar coupling between ^{6}Li and the nearby electronic spins allows high-resolution NMR spectra to be acquired with fewer spinning sidebands. A ^{6}Li MAS NMR variable-temperature study of *o*- and *m*-$LiMnO_2$ and *t*-$Li_2Mn_2O_4$ are presented in this work. The size of the shifts is rationalized in terms of a Fermi-contact shift mechanism, by considering the local environment surrounding the lithium cations. Nonideal paramagnetic behavior and possible magnetic ordering of the manganese, and the consequent implications for the Li hyperfine shift, are also examined.

Experimental Section

Sample Preparation. *o*-$LiMnO_2$ was prepared from Li_2CO_3 and MnO_2 by a conventional solid-state reaction. Stoichiometric amounts of the starting materials were mixed by grinding and then formed into pellets. The pellets were calcined under a flow of nitrogen gas at 650 °C for 6 h and then at 900 °C for 72 h with intermittent grindings. ^{6}Li-enriched samples of $^6LiMnO_2$, for the variable-temperature NMR experiments, were also prepared with ^{6}Li-enriched Li_2CO_3 (Isotec; ^{6}Li > 95%) as one of the starting materials, by using identical reaction conditions. *t*-$Li_2Mn_2O_4$ was prepared by intercalation of $LiMn_2O_4$ with excess *n*-BuLi.[12,13] $LiMn_2O_4$ was first synthesized by solid-state reaction of Li_2CO_3 and Mn_2O_3. The stoichiometric quantities were ground together, pelletized, and fired at 650 °C for 12 h and 850 °C for 24 h in air. The resulting $LiMn_2O_4$ was reacted with *n*-BuLi in anhydrous hexane at 20 °C for 12 h and 50 °C for 6 h under an N_2 atmosphere (sample I). Sample II was lithiated under more stringent conditions. The reaction vessel was evacuated

(14) Wills, A. S.; Raju, N. P.; Morin, C.; Greedan, J. E. *Chem. Mater.* **1999**, *11*, 1936.
(15) Greedan, J. E.; Raju, N. P.; Davidson, I. J. *J. Solid State Chem.* **1997**, *128*, 209.
(16) Ceder, G.; Mishra, S. K. *Electrochem. Solid-State Lett.* **1999**, *2*, 550.
(17) Singh, D. J. *Phys. Rev. B* **1997**, *55*, 309.
(18) Armstrong, A. R.; Gitzendanner, R.; Robertson, A. D.; Bruce, P. G. *Chem. Commun.* **1998**, 1833.
(19) Hwang, S.-J.; Park, H.-S.; Choy, J.-H.; Campet, G. *J. Phys. Chem. B* **2000**, *104*, 7612.
(20) Jang, Y.-I.; Chou, F. C.; Chiang, Y.-M. *J. Phys. Chem. Solids* **1999**, *60*, 1763.
(21) Lee, Y. J.; Wang, F.; Grey, C. P. *J. Am. Chem. Soc.* **1998**, *120*, 12601.
(22) Mustarelli, P.; Massarotti, V.; Bini, M.; Capsoni, D. *Phys. Rev. B* **1997**, *55*, 12018.
(23) Gee, B.; Horne, C. R.; Cairns, E. J.; Reimer, J. A. *J. Phys. Chem. B* **1998**, *102*, 10142.
(24) Sugiyama, J.; Hioki, T.; Noda, S.; Kontani, M. *J. Phys. Soc. Jpn.* **1997**, *66*, 1187.
(25) Treuil, N.; Labrugere, C.; Menetrier, M.; Portier, J.; Campet, G.; Deshayes, A.; Frison, J.-C.; Hwang, S.-J.; Song, S.-W.; Choy, J.-H. *J. Phys. Chem. B* **1999**, *103*, 2100.

first and then filled with N_2 gas (to a pressure of less than an atmosphere). The reactants were heated at approximately 50−60 °C for 24 h. The product was then washed with hexane and dried under vacuum. The layered *m*-$LiMnO_2$ was prepared by ion exchange from $NaMnO_2$.[6] The $NaMnO_2$ was first synthesized from Na_2CO_3 and Mn_2O_3 at 710 °C under an Ar atmosphere by a solid-state reaction. Then, $NaMnO_2$ and LiBr were refluxed in hexanol solution. The product was filtered, washed with alcohol, and dried. All products were then characterized with X-ray powder diffraction and the presence of the desired phases confirmed by comparing the powder patterns with those available in the Joint Committee on Powder Diffraction Standards (JCPDS).

Solid-State NMR Spectroscopy. ^{6}Li MAS NMR experiments were acquired on a CMX-200 spectrometer at an operating frequency for ^{6}Li of 29.45 MHz. Triple resonance Chemagnetics probes equipped with 4 mm rotors for MAS allowed spinning speeds of up to 16 kHz to be achieved, under variable temperature conditions. Spectra were recorded with either single-pulse or spin−echo ($90° - \tau - 180° - \tau$-acq.) pulse sequences. Because these echo experiments were performed under MAS conditions, the sequence was rotor synchronized, τ corresponding to one rotor period (1/spinning frequency). All spectra were referenced to 1 M LiCl solution at 0 ppm. A $\pi/2$ pulse of 2.8 μs was used with delay times of 0.5 s. The ^{6}Li longitudinal relaxation time (T_1) of the orthorhombic phase was measured with a spin inversion−recovery ($180° - \tau - 90°$-acq.) sequence. A Chemagnetics variable-temperature stack was used for the variable-temperature experiments. Temperature calibrations performed with $Pb(NO_3)_2$ showed a linear relation between the real and the indicated (i.e., measured) temperature, with differences of no more than 20 °C being observed at the extremes of temperatures investigated for the spinning speeds used. Real (calibrated) sample temperatures are given on the figures and throughout the text.

Results

The ^{6}Li MAS NMR room-temperature spectra of the *o*-, *m*- and *t*-$LiMnO_2$ phases are shown in Figure 1. Only one resonance at 36 and 143 ppm was observed for the *o*- and *m*-$LiMnO_2$ phases, respectively. Very weak resonances are observed at 76 and 5 ppm for *o*-$LiMnO_2$, which are tentatively assigned to the different lithium local environments that arise due to the stacking faults that are typically observed in this material.[26,27] A T_1 of 83 ms was measured for the resonance at 36 ppm in *o*-$LiMnO_2$. This is longer than the ^{6}Li T_1 value of 40 ms previously measured for the $LiMn_2O_4$ spinel.[21] For *t*-$Li_2Mn_2O_4$, different spectra were obtained depending on the synthesis conditions. A single resonance was observed at 99 ppm for the sample synthesized under N_2 atmosphere for a short reaction time (I), while two resonances at 101 and 118 ppm were observed for a second sample (II), which was prepared by reacting $LiMn_2O_4$ with *n*-BuLi for a longer time at a higher temperature. An intensity ratio of approximately 4:5 for the resonances at 118 and 101 ppm was obtained by deconvolution and integration of the resonances and their associated spinning sidebands. A resonance at 0 ppm was also observed for sample II, from a diamagnetic species. This is tentatively assigned to Li_2O or Li_2CO_3, possibly on the surface of the manganate particles.

The variable-temperature ^{6}Li MAS NMR spectra of *o*-$LiMnO_2$ are shown in Figure 2. No significant change

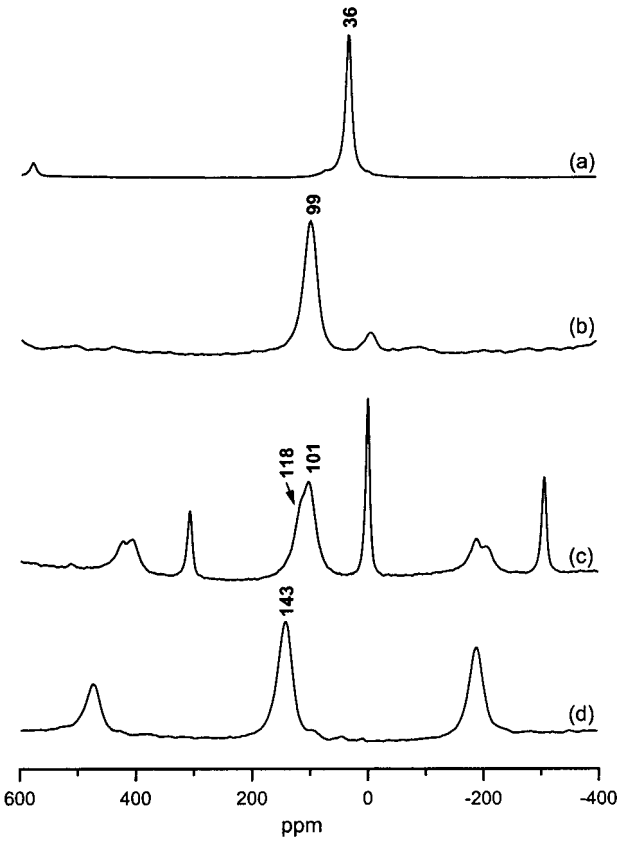

Figure 1. ^{6}Li NMR spectra of (a) *o*-$LiMnO_2$, (b) *t*-$Li_2Mn_2O_4$(I), (c) *t*-$Li_2Mn_2O_4$(II), and (d) *m*-$LiMnO_2$ acquired at room temperature. The spinning speeds used for (a), (b), (c), and (d) were 16, 15, 9, and 9.7 kHz, respectively. Spectrum (b) was acquired with an echo sequence, while the others were acquired with a one-pulse sequence. Isotropic resonances are marked on the spectra; all other peaks are spinning sidebands.

in the chemical shift position was observed for the temperature range of −28 to 283 °C. Significant line-broadening is observed in the spectrum acquired at −39 °C, accompanied by an increase in intensity of the spinning sidebands. In addition to the original resonance, which has now shifted to 32 ppm, a second resonance starts to appear at 5 ppm, together with a noticeable shoulder to lower frequency. As the temperature is lowered further to −66 °C, the resonance at ∼36 ppm disappears, leaving only a second resonance at −5 ppm. Only one resonance at −5 ppm is observed right down to the lowest temperature studied (−136 °C).

The ^{6}Li MAS NMR spectra of *t*- and *m*-$LiMnO_2$ as a function of temperature are shown in Figures 3 and 4, respectively. Considering t-$Li_2Mn_2O_4$ (sample I) initially, only one resonance at ∼99 ppm is visible between 176 and −136 °C. The spectra have been plotted in an absolute intensity mode, but changes in signal intensity due to the Boltzmann factor have not been accounted for. At 283 °C, two resonances at 85 and 118 ppm are seen for *t*-$Li_2Mn_2O_4$. The combined intensity of these two resonances is slightly less than the intensity of the resonance at 99 ppm at 176 °C. In contrast, the resonance at −1 ppm grows in intensity between 176 and 283 °C. A spectrum was then acquired for the sample after it had been slowly cooled back down close to room temperature (41 °C): only one resonance at ∼99 ppm (together with the resonance at −1 ppm) was observed, indicating that the temperature changes are

(26) Croguennec, L.; Deniard, P.; Brec, R.; Lecerf, A. *J. Mater. Chem.* **1997**, *7*, 511.
(27) Croguennec, L.; Deniard, P.; Brec, R.; Ricos, M. T. C.; Brohan, L. *Mol. Cryst. Liq. Cryst.* **1998**, *311*, 101.

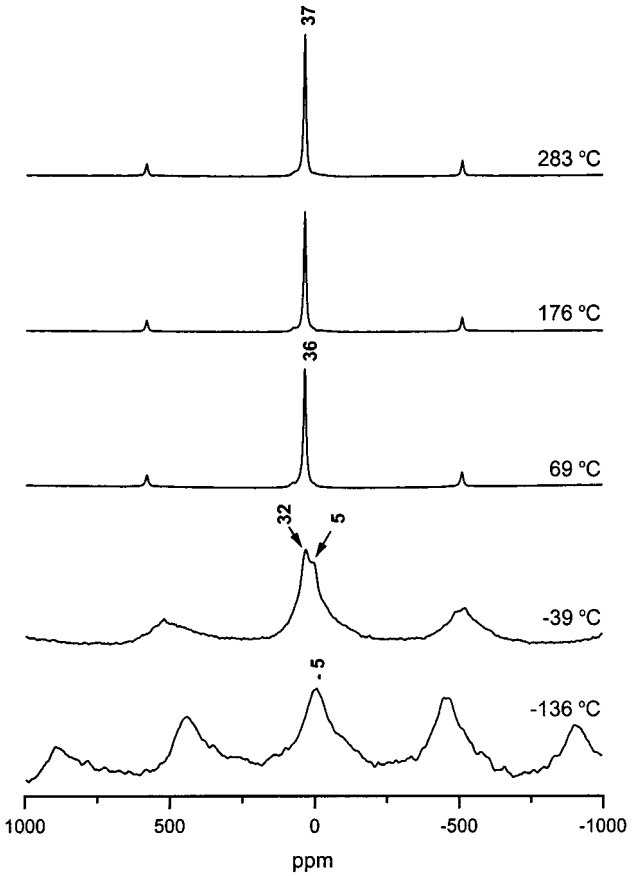

Figure 2. Variable-temperature ^{6}Li MAS NMR spectra of *o*-$LiMnO_2$ acquired at spinning speeds of 15−16 kHz with either one-pulse or a rotor-synchronized chemical-shift echo sequence ($\tau = 1$ rotor period). The real sample temperature, obtained by temperature calibration, is marked on the spectra. The same conditions were used to collect the spectra shown in Figures 3 and 4.

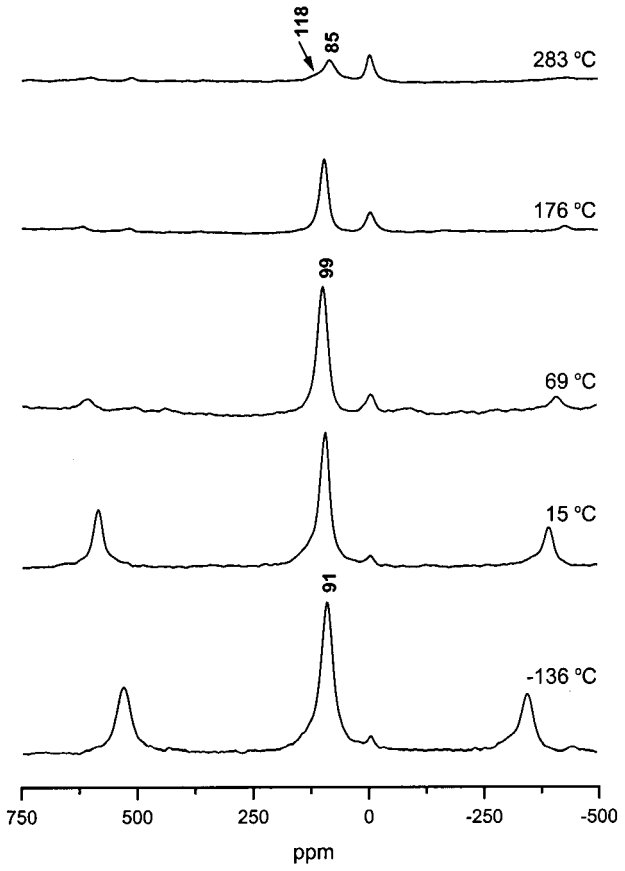

Figure 3. Variable-temperature ^{6}Li MAS NMR spectra of *t*-$Li_2Mn_2O_4$(I).

reversible. The ^{6}Li NMR resonance of *m*-$LiMnO_2$ slightly shifts to lower frequency as the temperature increases, shifting by 16 ppm over a 214 °C temperature range (Figure 4). At 283 °C, broad resonances at ∼381−455 ppm were observed in addition to the resonance at 113 ppm. When the temperature was lowered to 41 °C, two resonances were observed at 122 and 525 ppm, indicating that an irreversible change occurred.

Discussion

The ^{6}Li resonances of the Mn^{3+} (d^4) phases are observed at much lower frequencies than the ^{6}Li resonances of manganese oxides phases with manganese oxidation states of between +3.5 and +4. For example, resonances were previously observed at ∼500 ppm for $LiMn_2O_4$ ($Mn^{3.5+}$) and at ∼680 and ∼850 ppm for $Li_2Mn_4O_9$ and $Li_4Mn_5O_{12}$ (Mn^{4+}), respectively, due to lithium cations on the tetrahedral site of the spinel structure.[21] The lithium cations on the octahedral sites of the spinel structure give rise to a resonance at 1980 ppm for $Li_4Mn_5O_{12}$.[21] Thus, it is clear that the addition of an electron to the e_g orbital of manganese causes a shift to negative frequency. Furthermore, Curie−Weiss-like temperature dependences of the shifts were observed for $LiMn_2O_4$, and various transition metal (Ni^{2+}, Zn^{2+}, and Cu^{2+}) doped derivatives (i.e., a linear dependence between the shift, δ, and $1/T$ was observed).[21,28] No evidence for Curie−Weiss behavior is seen for the Mn^{3+} phases studied here. The mechanisms that are responsible for these shifts will now be considered, in order to rationalize these observations.

Shift Mechanisms. NMR spectra of paramagnetic materials are dominated by the interactions between unpaired electronic and nuclear spins. The three major interactions are the through-bond Fermi-contact interaction, through-space dipolar coupling, and the pseudo-contact interaction. The Fermi-contact interaction results from the unpaired electron spin density transferred from the paramagnet to the resonating nucleus via orbital overlap. The isotropic term part of the interaction is given by[29]

$$H_c = A_s I_z \langle S_z \rangle \quad (1)$$

where A_s is the hyperfine coupling constant and $\langle S_z \rangle$ is thermally averaged value of electronic spin. A_s depends on the nature and extent of the overlap between the orbitals containing the unpaired electrons and the s orbital at the nucleus of interest, the sign and the magnitude of this constant determining the direction and the size of the shift, respectively. Assuming that each nearby magnetic ion interacts independently with the nucleus, and that there are no interactions between the paramagnets, the Fermi-contact interaction will be

(28) Lee, Y. J.; Eng, C.; Grey, C. P. *J. Electrochem. Soc.* **2000**, in press.
(29) McConnell, H. M.; Robertson, R. E. *J. Chem. Phys.* **1958**, *29*, 1361.

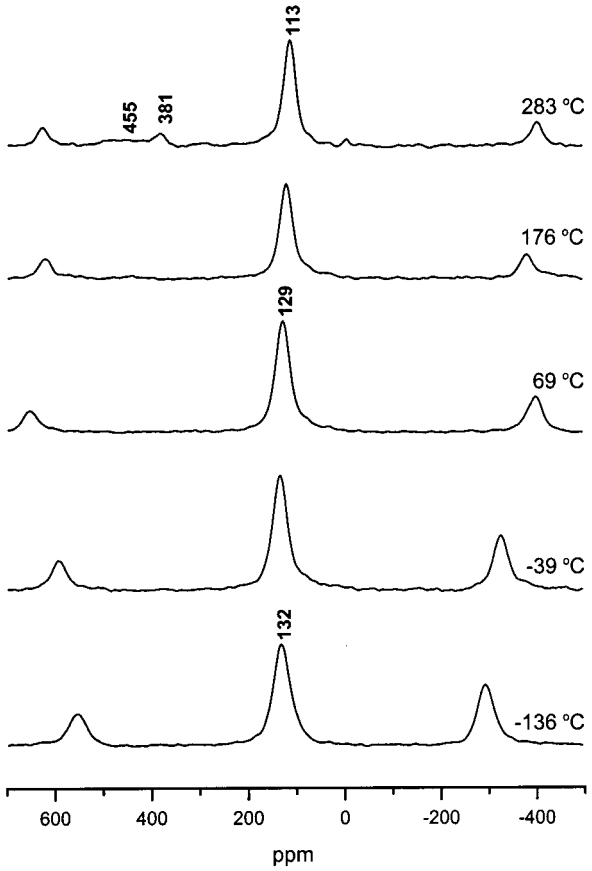

Figure 4. Variable-temperature ^{6}Li MAS NMR spectra of *m*-$LiMnO_2$.

additive and the total shift, δ, will be given by

$$\delta = \sum_i \frac{A_i}{\omega_0 \hbar} \langle S_z \rangle \tag{2}$$

The dipolar coupling is mediated by a through-space interaction between nuclear and electronic magnetic moment, and the Hamiltonian can be written as[30]

$$H_{en} = \bar{\mu}_e \cdot D_{en} \cdot \mu_N \tag{3}$$

where $\bar{\mu}_e$ is the time-averaged magnetic moment of electron and D_{en} is the dipolar coupling tensor. Coupling to an isotropic magnetic moment does not result in overall shift (under MAS), but instead is the major cause of the large spinning sideband manifolds and asymmetric line shapes often observed for paramagnetic solids. An anisotropic magnetic moment will lead to an isotropic pseudocontact shift, and for solids, to line-broadening. The shift is proportional to $1/r^3$ (r = electron−nuclear distance) and for a system with axial symmetry at the site of the paramagnet, $(3\cos^2\theta - 1)$ (where θ is the angle between the vector connecting the electronic and nuclear spins, and the principal axis of tensor that describes the anisotropy of the magnetic susceptibility).[31]

Lee et al.[21] and Mustarelli et al.[22] showed that the Li NMR shift in lithium manganese oxides spinels depends on the sum of the individual contributions from different

(30) Nayeem, A.; Yesinowski, J. P. *J. Chem. Phys.* **1988**, *89*, 4600.
(31) Kurland, R.; McGarvey, B. R. *J. Magn. Reson.* **1970**, *2*, 286.

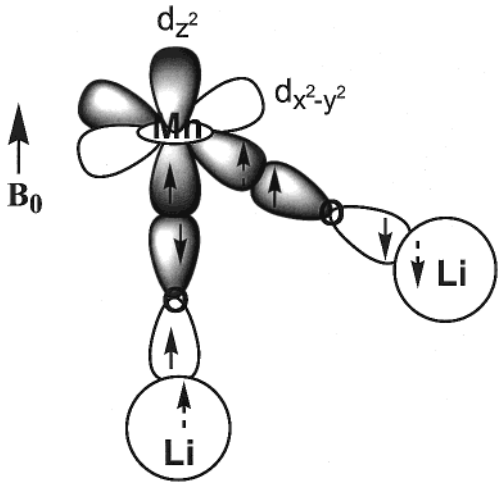

Figure 5. Schematic diagrams of transferred hyperfine interactions via Mn−O−Li 180° bonds. Electron spin density with the same sign is transferred from a half-filled d_z^2 orbital on the manganese atom to a Li 2s orbital, via an intervening oxygen atom. Spin density of an opposite sign results from the interaction involving an empty manganese $d_{x^2-y^2}$ orbital and the Li 2s orbital.

Li−O−Mn bonds and could not be directly correlated with the angle between the Mn−Li interatomic vector and principal axis of the atomic susceptibility tensor and the distance between lithium and manganese. Thus, it was proposed that the predominant factor affecting the Li NMR shift is the Fermi-contact interaction. The size and direction of the shifts observed for Mn^{4+} could then be readily rationalized by considering the Li−O−Mn angles and the extent of overlap between the t_{2g} orbitals and the intervening p orbitals on the oxygen atoms. Likewise, the Li NMR spectra of $LiMnO_2$ compounds are likely to be dominated by the Fermi-contact interaction, and this proposal will be discussed in more detail.

The molecular orbitals formed involving the manganese 3d, 4s, and 4p orbitals and the oxygen 2p orbitals of the MnO_6 octahedra are the $a_{1g}{}^b$, $e_g{}^b$, and $t_{1u}{}^b$ (bonding character), t_{2g} (nonbonding character), and $e_g{}^*$, $a_{1g}{}^*$, and $t_{1u}{}^*$ (antibonding character) orbitals. Because the $e_g{}^*$ orbital has an antibonding character, the addition of an electron to this orbital will cause an increase in the bond length between the manganese and oxygen atoms. Mn^{3+} cations have a high spin electron configuration ($t_{2g}{}^3e_g{}^1$) and the occupation of the doubly degenerate e_g level will lead to a Jahn−Teller distortion, resulting in an elongation of the two Mn−O bond lengths oriented in the same direction as the occupied $3d_z^2$ orbital. When the d_z^2 orbital is half-filled and the $d_{x^2-y^2}$ orbital is empty, the 180° interaction between a manganese $d_{x^2-y^2}$ orbital and a Li 2s orbital will result in the transfer of negative electron spin density through the intervening oxygen orbital, and thus in a negative shift (Figure 5). In contrast, electron spin density with the same sign will be transferred to the Li 2s orbital from the filled manganese d_z^2 orbital (Figure 5).

The Li NMR shifts in the lithium manganates may be rationalized by considering the local structure surrounding the lithium cations in the different phases (refer to Table 1). The lithium site in *o*-$LiMnO_2$ is connected to the first cation-coordination sphere via 12 Li−O−Mn bonds with 90° bond angles, 4 Li−O−Mn 180° bonds, and 2 Li−O−Li 180° bonds. The manganese

Table 1. Local Environment for Lithium and the Li NMR Shifts of the Mn^{3+} Compounds

compound	space group	site for Li	no. of Li−O−Mn bonds	bond angle	NMR shift (ppm)
o-$LiMnO_2$	*Pmmn*	2a	12	90°	36
			4	180° Mn(e_g^0)	
			0	180° Mn(e_g^1)	
m-$LiMnO_2$	*C*2/*m*	2d	12	90°	∼129−143
			4	180° Mn(e_g^0)	
			2	180° Mn(e_g^1)	
t-$Li_2Mn_2O_4$ (I)	$I4_1/amd$	8c	12	90°	99
			4	180° Mn(e_g^0)	
			2	180° Mn(e_g^1)	
t-$Li_2Mn_2O_4$ (II)	$I4_1/amd$	4a	12	122.3°	118
		8c	12	89.9°	101
			6	176.7°	

atom in this structure contains four short Mn−O bonds (1.92−1.94 Å) and two longer ones (2.30 Å). The shorter bonds are involved in the Li−O−Mn 180° interactions, indicating that the e_g orbital pointing along the directions of the four O−Mn bonds is not occupied, and may be assigned to a $d_{x^2-y^2}$ orbital. *m*-$LiMnO_2$ and *t*-$LiMnO_2$ have the same Li local environments, both containing 12 Li−O−Mn 90° interactions, 4 Li−O−Mn 180° interactions involving short Mn−O bonds, and 2 Li−O−Mn 180° interactions involving longer Mn−O bonds, and thus half-filled d_z^2 orbitals. The similar NMR shifts observed for *m*-$LiMnO_2$ (∼143 ppm) and *t*-$LiMnO_2$ (∼99−101 ppm) are consistent with their similar local environments. The much smaller shift for *o*-$LiMnO_2$ (36 ppm) is consistent with the lack of Li−O−Mn 180° interactions involving occupied e_g orbitals, which should result in large positive shifts, and suggests that each Li−O−Mn (e_g^1) 180° interaction results in a mean shift of approximately +50 ppm.

Clearly, the interactions with the t_{2g} electrons must contribute to the total shift, and are, in the case of *o*-$LiMnO_2$, responsible for a positive overall shift observed for this compound. In our previous paper, it was shown that a 90° Li−O−Mn interaction involving half-filled t_{2g} orbitals results in a shift of approximately 150 ppm per Li−O−Mn interaction, in Mn(IV) compounds. On this basis, a contribution to the shift of 1800 ppm from the interactions with the t_{2g} electrons is predicted for the three Mn(III) compounds. Although smaller hyperfine interactions may be expected for the more ionic Mn(III) compounds, in comparison to those for the Mn(IV) compounds,[23] this cannot be the only cause of the much smaller shifts observed in the Mn(III) compounds. We ascribe the smaller shifts to residual electron−electron correlations and, hence, reduced $\langle S_z \rangle$ values for these compounds.

Irregular Temperature Behavior and Magnetic Ordering. Because $\langle S_z \rangle$ in eq 1 is proportional to χB_0 through the equation[32]

$$\langle S_z \rangle = -\frac{B_0}{\mu_0 g N_0 \mu_B}\chi \qquad (4)$$

the Fermi-contact interaction should show the same temperature behavior as the magnetic susceptibility χ. (In eq 4, μ_0 denotes the permeability, g is the electron g-factor, N_0 is Avogadro's number, and μ_B is the Bohr magneton.) For example, as discussed previously, the ^6Li and ^7Li NMR shifts of $LiMn_2O_4$ are inversely proportional to temperature above room temperature, with a Curie-like behavior.[21] This is consistent with the magnetic susceptibility of this compound, which has been observed, by one group, to follow Curie−Weiss behavior above 40 K. A slight change in the slope of $1/\chi$ vs T at 256 K was noted, however, due to the Jahn−Teller distortion.[24] Wills et al. also reported that the spinel $LiMn_2O_4$ shows a Curie−Weiss behavior above the Jahn−Teller distortion temperature (∼290 K), the spin frustration causing a depression of antiferromagnetic transition temperature (∼45 K) with respect to the Weiss constant (−300 K).[33] In contrast, the ^6Li NMR shifts of Mn^{3+} compounds are essentially independent of temperature up to 283 °C. This is, however, consistent with the magnetic susceptibility data for these compounds. The susceptibility data reveal very broad maxima in χ at 360, 120, and 250 K for *o*-$LiMnO_2$,[15] *t*-$Li_2Mn_2O_4$,[14] and *m*-$LiMnO_2$,[8] respectively, indicating the presence of short-range magnetic ordering in these temperature regimes. Curie−Weiss behavior was not observed until above 600 K for both *o*- and *t*-$LiMnO_2$.[14,15] These temperature dependences are consistent with the dominance of short-range 2-D electronic correlations with antiferromagnetic ordering of the manganese spins. The small changes in shift are readily rationalized: the shifts of *t*-$Li_2Mn_2O_4$ and *m*-$LiMnO_2$ actually increase slightly as the temperature is increased from −136 to ∼69 °C (for *t*-$Li_2Mn_2O_4$) and −39 °C (for *m*-$LiMnO_2$), which is ascribed to the reduction of the short-range correlations and, thus, a slight increase in χ in this regime. The shift remains approximately constant from 69 to 176 °C for *t*-$Li_2Mn_2O_4$ and between 69 and 283 °C for *o*-$LiMnO_2$, presumably due to a similar temperature dependence of the two competing trends in these temperature regimes, namely: (i) a reduction in χ due to increased population of the higher energy Zeeman (electronic) states (this will result in a smaller hyperfine shift), and (ii) the reduction of the short-range electronic correlations (this will lead to a larger hyperfine shift), as the temperature increases. The shift of *m*-$LiMnO_2$ decreases from 69 to 283 °C, as the first term dominates and the regime where Curie−Weiss behavior has been reported is approached. A maximum δ is reached for *o*-$LiMnO_2$ at a higher temperature than the maxima of the *t*- and *m*-phases, which is consistent with its maximum in χ, which also occurs at the highest temperature. Unlike the previously reported susceptibility data for *t*-$Li_2Mn_2O_4$, however, the maximum in δ is observed at approximately 200 °C higher than the maximum in χ. We ascribe this to small differences in sample preparations and local ordering.

o-$LiMnO_2$ undergoes a magnetic phase transition at 261.5 K from short-range 2-D correlations to 3-D long-range ordering.[15] Assuming that the Mn electronic spins are oriented along the *a*-axis, and that antiferromagnetic coupling between the planes occurs below the transition temperature, as shown in the neutron diffraction study, only one magnetically inequivalent site for lithium can be identified in the 2a × 2b × 2c

(32) Drago, R. S. *Physical Methods for Chemists*; Harcourt Brace Jovanovich: New York, 1992.

(33) Wills, A. S.; Raju, N. P.; Greedan, J. E. *Chem. Mater.* **1999**, *11*, 1510.

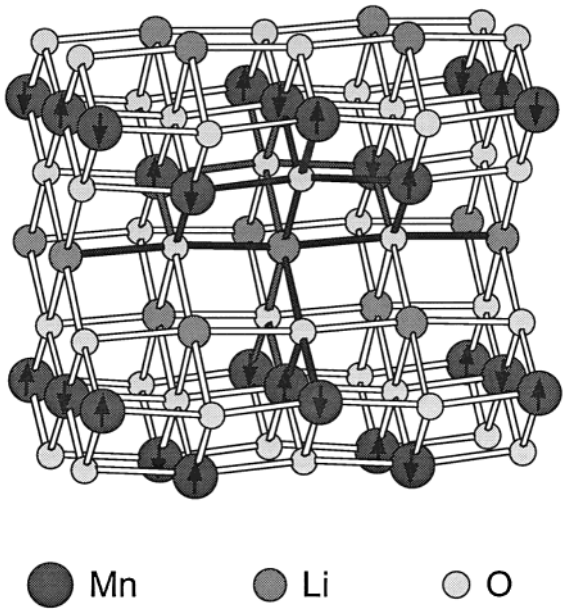

Figure 6. The local coordination environment of the lithium cation in the *o*-$LiMnO_2$ structure with 3-D antiferromagnetic spin correlations. The Li−O−Mn bonds involving the central lithium cation are shaded.

magnetic unit cell.[15] The lithium cation is coordinated to three "spin-up" Mn ions and three "spin-down" Mn ions through 90° Li−O−Mn bonds, and two "spin-up" and two "spin-down" Mn ions as second nearest neighbors via 180° Li−O−Mn bonds (Figure 6). Therefore, the total spin density transferred to the lithium cations from the manganese ions will be canceled out and a Li hyperfine shift of 0 ppm is predicted. Thus, the resonance at −5 ppm is assigned to the Li cation in a 3-D coupled antiferromagnet. The large increases in spinning sideband intensity and line width are assigned to the presence of the large internal fields inside this material. Two resonances are observed at −39 °C, presumably due to incomplete long-range ordering at this temperature.

Previous local spin density approximation (LDA) calculations have suggested that the manganese ions in *m*-$LiMnO_2$ are coupled antiferromagnetically along the *b*-axis and that the correlations between the layers are very weak, resulting in the probable suppression of long-range order even down to low temperatures.[17] ^{6}Li NMR spectra of *m*-$LiMnO_2$ do not show any evidence for the magnetic phase transition as the temperature decreases, consistent with this suggestion. Assuming that *m*-$LiMnO_2$ adopts AF3 type antiferromagnetic ordering in the layers and antiferromagnetic coupling between the layers, as suggested from the theoretical calculations of Singh,[17] two (magnetically) inequivalent local environments for lithium cations can be distinguished: one coordinated to 2 Mn (spin-up, ↑) and 4 Mn (spin-down, ↓) via 90° Li−O−Mn bonds and 6 Mn (↑) via 180° Li−O−Mn bonds and a second with 4 Mn (↑), 2 Mn (↓) through 90° Li−O−Mn bonds and 6 Mn (↓) via 180° Li−O−Mn bonds. However, only one ^{6}Li resonance at ∼130 ppm is observed even down to −136 °C, indicating the absence of 3-D long-range magnetic ordering, even at this temperature.

NMR spectroscopy is a technique associated with a relatively long time scale (typically, 10^{-2}−10^{-6} s); thus, in order to observe discrete magnetically inequivalent lithium spins, or linebroadening of the NMR line shape (from this interaction), the electron−electron correlations must be associated with time scales in or longer than this regime; this is clearly the case for *o*-$LiMnO_2$ below the Néel temperature. Antiferromagnetic correlations with shorter time scales will result in single lithium resonances (e.g., in the ^{6}Li spectra of *t*-$Li_2Mn_2O_4$) with shifts that should gradually approach the average of the shifts observed in the antiferromagnetic (AF) state, as the AF correlations increases (as seen for *o*-$LiMnO_2$ just above the Néel temperature). Thus, in principle, information concerning the time scales of the magnetic moment spin−spin fluctuations could, in certain regimes, be extracted from the NMR line shapes. Furthermore, unlike magnetic susceptibility measurements, which can be used to measure the reduction of the time-averaged magnetic moments for the bulk sample due to the AF interactions, (high resolution) NMR should also provide a spatial probe of these interactions. This will be explored in more detail in a subsequent publication.

Phase Transitions of *t*-$Li_2Mn_2O_4$ and *m*-$LiMnO_2$ at High Temperatures. No structural changes were observed by NMR for *o*-$LiMnO_2$ at high temperatures. However, *m*-$LiMnO_2$ and *t*-$Li_2Mn_2O_4$ both show changes in their NMR spectra at 283 °C, which appear to be related to structural changes. The spectrum of *t*-$Li_2Mn_2O_4$ (sample I) at 283 °C (Figure 3) is similar to the spectrum of sample II at room temperature (Figure 1): two resonances at ∼85 and ∼118 ppm along with a resonance at close to 0 ppm are observed in both spectra. As discussed previously, there has been some debate as to the site occupied by lithium during the insertion of lithium ion into spinel $LiMn_2O_4$. David et al. obtained site occupancies of 43 and 79%, for the 4a tetrahedral site and 8c octahedral sites, respectively,[13] whereas Wills et al. obtained a full occupancy of the 8c site[14] in two different neutron diffraction studies. Recent first principles calculations showed that the lithium cation is gradually displaced from the tetrahedral site to the octahedral site as the lithium concentration is raised above $x = 1$ ($Li_xMn_2O_4$), resulting in the predominant occupancy of the octahedral sites at $x \approx 2$.[34] This study also predicted that the occupation of tetrahedral site by lithium will increase with temperature, because of thermal excitations. Therefore, it is possible that the distribution of lithium between the two sites might differ between compounds, depending on the synthesis conditions. Considering the multiplicity of the two crystallographic sites, the ratio of the concentration of lithium residing in the tetrahedral to octahedral site, obtained in the first neutron diffraction study, is 3:11.[13] Our NMR spectrum of sample II shows two resonances with the intensity distribution of 4:5. Therefore, the more intense resonance at 101 ppm is assigned to lithium in 8c octahedral site and the less intense resonance at 118 ppm to 4a tetrahedral site. The migration of lithium cations into tetrahedral sites at high temperatures, seen in sample I, is reversible: when the temperature is lowered down to 41 °C, only one ^{6}Li resonance at 99 ppm is observed, from lithium cations

(34) Van der Ven, A.; Marianetti, C.; Morgan, D.; Ceder, G. *Solid State Ionics* **2000**, in press.

residing in the octahedral site only. These ^{6}Li NMR results suggest that the structure with lithium residing on both the 4a and 8c sites is less energetically favorable, but may be synthesized with more stringent synthesis conditions.

One other possible assignment of the two resonances at 101 and 118 ppm that should be considered is that they arise from an electronic rather than structural differences in the lithium local environment. It appears extremely unlikely, however, that two inequivalent sites should be created at high temperatures, rather than at low temperatures, where some long-range ordering might be expected.

Considering the high-temperature spectra of *m*-$LiMnO_2$, where new resonances at 380 to 500 ppm and −3 ppm begin to appear at 283 °C, the stability of this compound was investigated and it was shown that *m*-$LiMnO_2$ is transformed into a mixture of *o*-$LiMnO_2$, $Li_2Mn_2O_4$, and $LiMn_2O_4$ above ∼300 °C.[7] We previously observed a ^{6}Li NMR shift at ∼390 ppm for the stoichiometric spinel $LiMn_2O_4$ at 283 °C,[21] thus the resonance at 381 ppm in Figure 4 is assigned to this phase. The resonance at ∼455 ppm is most likely due to a manganate phase with an even higher oxidation state, and is tentatively assigned to a spinel material containing defects. The resonance at −3 ppm can be assigned to diamagnetic lithium cations, produced by the decomposition of $LiMnO_2$ to form $LiMn_2O_4$. The NMR spectrum obtained at 41 °C after the variable-temperature experiment shows that the decomposition is irreversible: the resonance at 525 ppm, with low intensity, is assigned to the spinel phase and the resonance at 122 ppm is assigned to *m*-$LiMnO_2$. Therefore, it is clear that *m*-$LiMnO_2$ is a metastable phase, which decomposes into the spinel phase $LiMn_2O_4$. Further studies at higher temperatures could not be performed because of the limits of our high-temperature NMR equipment.

Conclusions

Discrete ^{6}Li NMR resonances were observed for lithium manganese oxides containing manganese with an oxidation state of +3. Much smaller NMR shifts are seen for *o*-$LiMnO_2$, *t*-$Li_2Mn_2O_4$, and *m*-$LiMnO_2$ at 36, 99, and 143 ppm, respectively, in comparison to the hyperfine shifts for lithium manganese oxide spinels with manganese oxidation states from +3.5 to +4 (from 500 to 1980 ppm). The NMR shifts of these materials are dominated by the Fermi-contact interaction, which is sensitive to the local structure surrounding a lithium cation. The NMR spectra of o-$LiMnO_2$ show no dependence on temperature from −28 to 283 °C, indicating non-Curie paramagnetism due to short-range antiferromagnetic couplings between manganese spins. At lower temperatures, a second resonance with a very small or negligible hyperfine shift appears and the original resonance gradually decreases in intensity, and finally disappears. This is ascribed to a magnetic phase transition from 2-D short-range correlations to 3-D long-range antiferromagnetic ordering and indicates that high-resolution spectra may be obtained from systems below the Néel temperature. The ^{6}Li NMR shifts for *t*-$Li_2Mn_2O_4$ and *m*-$LiMnO_2$ remain approximately constant from −136 to 176 °C, which is also ascribed to the short-range antiferromagnetic electronic correlations. However, no evidence for long-range ordering was observed.

The lithium tetrahedral site in the tetragonal structure is populated in materials synthesized with more stringent synthesis conditions. For materials synthesized at lower temperatures, however, only the octahedral site is populated at room temperature, but at 283 °C, the highest temperature studied, two resonances are observed due to lithium cations on tetrahedral and octahedral sites. The metastable phase *m*-$LiMnO_2$ undergoes an irreversible decomposition to *o*-$LiMnO_2$ and the spinel phase at high temperatures and resonances due to Li^+ in both normal and defect spinels phases were observed at 283 °C.

Finally, this work has shown that in nondilute paramagnetic systems, it may not always be possible to rationalize the hyperfine shift by treating the ions as individual paramagnets and ignoring coupling between these spins. Non-Curie Law behavior of the ^{6}Li hyperfine shift appears to be a characteristic of these electronic correlations. Thus, it should be possible to use this temperature dependence in more complex materials to characterize, or as a signature of, lithium local environments containing magnetically coupled spins. Extensions of this approach to a series of transition metal oxides are currently underway.

Acknowledgment. This work was performed with support from the National Science Foundation (DMR 9901308).

CM000469T